Pergamon

Acta mater. 48 (2000) 3745–3759

Acta MATERIALIA

www.elsevier.com/locate/actamat

CRYSTALLOGRAPHY AND STRUCTURAL EVOLUTION OF CUBIC BORON NITRIDE FILMS DURING BIAS SPUTTER DEPOSITION

D.V. SHTANSKY*[1]†, O. TSUDA[2], Y. IKUHARA[1] and T. YOSHIDA[2]

[1]Engineering Research Institute, School of Engineering, The University of Tokyo, 2-11-16 Yayoi, Bunkyo-ku, Tokyo 113-8656, Japan, [2]Department of Metallurgy and Materials Science, Graduate School and Faculty of Engineering, The University of Tokyo, 7-3-1 Hongo, Bunkyo-ku, Tokyo 113-8656, Japan

(Received 8 February 2000; received in revised form 22 May 2000; accepted 22 May 2000)

Abstract—The mechanism and the crystallography of the growth of cubic boron nitride (c-BN) films deposited on ⟨100⟩-oriented silicon substrates by radio-frequency bias sputtering have been studied by means of cross-sectional high-resolution transmission electron microscopy. Particular attention has been paid to the atomic structure of graphitic (sp^2-bonded) BN and grain boundaries in the c-BN films. The c-BN films grow in the sequence of amorphous boron nitride (a-BN), turbostratic boron nitride (t-BN) and c-BN layers, similar to previous results. The sp^2-bonded BN material consists of small regions, 1–5 nm thick, forming in a layered manner parallel to the substrate surface. Each region consists of parallel lamellae in both the hexagonal and rhombohedral (h-BN and r-BN, respectively) configurations. Three orientation relationships between h-BN and r-BN phases were determined: OR-1: $[2\bar{1}10]_{h\text{-}BN}\|[2\bar{1}10]_{r\text{-}BN}$, $(0001)_{h\text{-}BN}\|(0001)_{r\text{-}BN}$; OR-2: $[2\bar{1}10]_{h\text{-}BN}\|[2\bar{1}10]_{r\text{-}BN}$, $(0\bar{1}10)_{h\text{-}BN}\|(0\bar{1}\bar{1}1)_{r\text{-}BN}$; OR-3: $[2\bar{1}10]_{h\text{-}BN}\|[2\bar{1}10]_{r\text{-}BN}$, $(0\bar{1}10)_{h\text{-}BN}\|(01\bar{1}2)_{r\text{-}BN}$. The r-BN crystallites within the sp^2-bonded BN grow preferentially in such a way that the $(01\bar{1}2)_{r\text{-}BN}\|(0\bar{1}11)_{r-BN}$ plane is almost parallel to the grain boundary. Twinning about both the basal planes and the $\{0\bar{1}11\}_{r\text{-}BN}$ planes is common within r-BN phase. The c-BN crystallites adjacent to the graphitic BN layer are highly twinned, the $\{\bar{1}\bar{1}1\}_{c\text{-}BN}$ twin planes being parallel to the basal planes of the sp^2-bonded BN. The c-BN phase nucleates on the oriented graphitic BN layer in a semicoherent manner and obeys specific orientation relationships with the hexagonal and rhombohedral phases, namely:

OR-I: $[\bar{2}110]_{r\text{-}BN}\|[110]_{c\text{-}BN}$
$(01\bar{1}\bar{1})_{r\text{-}BN}\|(\bar{1}\bar{1}1)_{c\text{-}BN}$ (interface plane)
$(0001)_{r\text{-}BN}\approx\|(1\bar{1}\bar{1})_{c\text{-}BN}$

OR-II: $[\bar{2}110]_{r\text{-}BN}\|[\bar{1}\bar{1}0]_{c\text{-}BN}$
$(01\bar{1}2)_{r\text{-}BN}\|(1\bar{1}\bar{1})_{c\text{-}BN}$ (interface plane)
$(0001)_{r\text{-}BN}\approx\|(1\bar{1}\bar{1})_{c\text{-}BN}$

They are related by a rotation of 180° about their common axis, $[0001]_{r\text{-}BN}\|[1\bar{1}\bar{1}]_{c\text{-}BN}$,

$$[2\bar{1}\bar{1}0]_{h\text{-}BN}\|[110]_{c\text{-}BN}$$
$$(0\bar{1}12)_{h\text{-}BN}\|(00\bar{1})_{c\text{-}BN}$$
$$(0001)_{h\text{-}BN}\|(\bar{1}\bar{1}\bar{1})_{c\text{-}BN}$$

In the mainly c-BN region of the films, twins are present about more than one of the sets of $\{\bar{1}\bar{1}1\}_{c\text{-}BN}$ planes. The intrinsic microstructure of the c-BN films and the crystallography between the cubic and graphitic BN phases show that the structure of cubic boron nitride is directly related to the structure of the precursor phases. The atomic structure of an interface depends on the orientation relationship between adjacent c-BN grains and the boundary inclination. The grain boundaries consist of twin boundaries when two adjacent grains are oriented close to the $[110]_{c\text{-}BN}$ zone axis and the boundary plane is parallel to the $\{\bar{1}\bar{1}1\}_{c\text{-}BN}$ close-packed planes of both grains. However, a thin layer, 1–2 nm, of sp^2-bonded BN forms between the c-BN grains when the boundary plane inclines a few degrees from the $\{\bar{1}\bar{1}1\}_{c\text{-}BN}$ planes of the adjacent grains. © *2000 Acta Metallurgica Inc. Published by Elsevier Science Ltd. All rights reserved.*

Keywords: Physical vapor deposition (PVD); Nucleation, growth; Thin films; Transmission electron microscopy (TEM); Microstructure

1. INTRODUCTION

Cubic boron nitride (c-BN) thin films are of interest because of their excellent physical, chemical and mechanical properties. Thus the available literature is extensive, covering many different aspects of c-BN thin film deposition such as microstructure [1–10], stress and strain fields [11–13], effect of ion bombardment [14, 15], crystallographic texture [16–19], substrate effects [20, 21], surface morphology [22], growth mechanisms (momentum transfer model [14,15,23], compressive stress model [11], subplantation model [24–27], selective sputter model [28]),

* On leave from the I.P. Bardin Iron and Steel Industry Institute, 2nd Baumanskaya Street, 9/23, Moscow 107005, Russia.

† To whom all correspondence should be addressed.

1359-6454/00/$20.00 © 2000 Acta Metallurgica Inc. Published by Elsevier Science Ltd. All rights reserved.
PII: S1359-6454(00)00159-2

and mechanical properties [9]. Both ion-assisted physical vapor deposition (PVD) and chemical vapor deposition (CVD) techniques have been used successfully in a large number of studies. A complete review of experimental results related to the deposition of c-BN thin films was compiled by Hackenberger *et al.* [29] and recently supplemented by Yoshida [30, 31]. It has been shown that energetic ion bombardment [32–35] resulting in high compressive stresses of several GPa [11, 13] is needed for the deposition of c-BN films. It has been suggested that the stress induces the c-BN formation [11]. c-BN films typically grow with a layered structure consisting of an amorphous layer at the film/substrate interface, followed by preferentially oriented sp^2-bonded BN, and a final layer of c-BN. This layered structure seems to be independent of the deposition process.

Although previous research has been comprehensive, a number of problems still remain unsolved. Whilst several c-BN deposition models are available [11,14,15,23–28], there are still disagreements concerning the mechanism and the crystallography of c-BN nucleation and growth. McKenzie and co-workers [18, 36] suggested that the texture of the hexagonal boron nitride (h-BN) and c-BN layers arises because these textures minimize the thermodynamic (Gibbs) free energy for a given biaxial compressive stress field, whereas Cardinale *et al.* [12] and McCarty [17] argued that the textures observed are not those that minimize elastic strain energy. They suggested that the c-BN texture observed arises directly from the growth mechanism. Recently, Zeitler *et al.* [13] showed that the stress evolution is characterized by high tensile stress in the initial stage of BN film growth, followed by a transition from tensile to compressive stress, which is connected with formation of the c-BN phase. Ballal *et al.* [19] found that c-BN films were preferentially oriented with the [110] axis normal to the substrate surface, but neither Kester *et al.* [3] nor Medlin *et al.* [5] reported a similar preferential orientation of the c-BN. In contrast, the analysis by Medlin and co-workers indicates that c-BN films grow with [111] in-plane orientation, resulting in a crystallographic alignment between the basal planes of the turbostratic boron nitride (t-BN) and the {111} planes of c-BN. A strong correlation between $\{003\}_{r\text{-}BN}$ and $\{111\}_{c\text{-}BN}$ planes, and between $\{101\}_{r\text{-}BN}$ and $\{111\}_{c\text{-}BN}$ planes (where r-BN indicates rhombohedral phase), has been shown by Yamada-Takamura *et al.* [10]. However, it is still unclear whether the r-BN phase acts as a structural precursor or a preferred nucleation site for the c-BN phase. Medlin *et al.* [5] observed twinning about a single type of {111} plane within any individual c-BN crystallite, whereas in diamond films, twinning about more than one set of the {111} planes within a grain has been reported [37–39]. The reason for this discrepancy is not clear at present.

While the orientation dependence of elastic strain energy in the hexagonal BN layer has recently been debated [12,17,18,36], little is known regarding the structure of the graphitic (sp^2-bonded) BN layer. The sp^2-bonded BN is highly disordered and is usually described as turbostratic BN [40], with hexagonal sheets roughly parallel to each other but randomly rotating about the layer normal. Thus, it is believed that the sp^2-bonded material is in the hexagonal configuration although evidence for the presence of r-BN has been recently observed [4, 10]. It is thus questionable whether h-BN is the dominant phase in the t-BN layer. The atomic structure of the grain boundaries in the sp^2-bonded BN has not been studied.

The grain size of PVD c-BN films is extremely small, 5–20 nm [7, 8], which is typical for nanocrystalline materials (NM). The structure of the grain boundaries, the volume fraction of which is extremely large in NM, plays an important role in the microscopic properties of a material. There is still disagreement concerning the structure of the grain boundaries in c-BN films. For example, Ichiki *et al.* [22] observed twin boundaries denoted $\Sigma 3$ types, whereas Zhou *et al.* [8] reported the h-BN phase at the boundaries between c-BN crystallites. It is also speculated that once the growth of cubic phase is initiated, the c-BN phase grows without further transformation [3, 30].

In the present study, high-resolution transmission electron microscopy (HRTEM) was used to reveal the crystallography and the structural evolution of c-BN films synthesized using radio-frequency (RF) bias sputtering. Particular attention has been paid to the structure of grain boundaries in the cubic and graphitic BN layers.

2. EXPERIMENTAL PROCEDURE

c-BN films were deposited on ⟨100⟩-oriented silicon wafers by RF bias sputtering [41] using a sintered hexagonal BN target. Prior to deposition, the substrates were sputter cleaned by ionic etching in argon at a bias voltage of -90 V for 15 min. The parameters of the deposition process and some film characteristics are shown in Table 1. Thin foils for cross-sectional high-resolution TEM studies were prepared by a standard technique involving mechanical grinding, followed by mechanical dimpling and ion milling to perforation. The structure of the films was examined in a Hitachi-9000NAR transmission electron microscope with a point resolution of 0.19 nm operating at 300 kV. HRTEM was performed by tilting the film/substrate interface into an exact $[110]_{Si}$ zone-axis orientation. The simulation of HRTEM images and interface modeling were computed with MacTempas and CrystalKit software packages, with spherical aberration coefficient of the objective lens 0.85 mm, half-width of a Gaussian spread of focus due to chromatic aberration 6.5 nm, semi-angle of

Table 1. Sputtering regimes and coating characteristics

No.	Target power (W)	Bias voltage (V)	Deposition time (min)	Sputtering gas	Thickness (nm)	Structure[a]	c-BN grain size (nm)
1	1000	−150	8	Ar	>400	a-BN, t-BN, c-BN	–
2	1000	−300	4	Ar	65	a-BN, t-BN, c-BN	5–12
3	2000	−300	3	Ar	115	a-BN, t-BN, c-BN	2–12
4	1000	−400	8	Ar	65	a-BN, t-BN	–

[a] a-, t- and c-BN indicate amorphous, turbostratic and cubic BN, respectively.

incident beam convergence 0.65 mrad, and effective aperture 10 nm^{-1}.

3. EXPERIMENTAL RESULTS

3.1. Structure of sp²-bonded BN

The characterization of sp^2-bonded BN is particularly difficult because h-BN and r-BN differ only in the stacking sequence of the basal planes, the *d* spacing of the hexagonal planes being the same (hereafter, the r-BN crystal is referenced to the hexagonal indexing system). The dominant fringe contrast, which is usually observed in the image of sp^2-bonded BN, arises from basal planes that are oriented edge-on. In h-BN phase, every other layer is rotated by 180° around the [0001] direction, whereas in r-BN phase, all layers have the same rotation sense but are successively displaced relative to each other by a vector of $a/3$ in a $\langle 01\bar{1}0\rangle$ direction, resulting in a three-layer stacking sequence. Medlin *et al*. [4] showed that it is possible to observe the atomic arrangement within the basal planes of both phases if the specimen is aligned sufficiently well with a $\langle 2\bar{1}\bar{1}0\rangle$ direction. In h-BN phase, the (0002) and $(10\bar{1}0)$ planes are orthogonal, whereas in r-BN, the angle θ_1 between (0003) and $(10\bar{1}\bar{0})$ planes and the angle θ_2 between (0003) and $(01\bar{1}2)$ planes can be expressed as follows

$$\tan\theta_1 = 2c/\sqrt{3}a,\ \tan\theta_2 = c/\sqrt{3}a.$$

Using the convention a=0.2504 nm and c=1.00 nm (card No. 45-1171, JSPDS), these angles are 77.7° and 66.5°, respectively.

The microstructure of sp^2-bonded BN was studied in film 2. Fig. 1(a) shows a cross-sectional HRTEM image of a typical area of sp^2-bonded BN taken 14 nm away from the film/substrate interface. The incident beam is close to $[2\bar{1}\bar{1}0]$. Fig. 1(b) is a schematic key diagram showing angles between the lines of intense white points within the region surrounded by a white square frame. It can be seen that the sp^2-bonded material consisted of parallel lamellae in both the h-BN and r-BN configurations, the basal planes being parallel. The orientation relationship between the hexagonal and rhombohedral phases can be expressed as follows

$$\text{OR-1:}\ [2\bar{1}\bar{1}0]_{\text{h-BN}}\|[2\bar{1}\bar{1}0]_{\text{r-BN}}$$
$$(0001)_{\text{h-BN}}\|(0001)_{\text{r-BN}}$$

[Hereafter, the basal planes of r-BN and h-BN phases will be denoted as (0001).] Note that, across the interface, $(01\bar{1}\bar{1})_{\text{r-BN}}$ and $(01\bar{1}0)_{\text{h-BN}}$ planes were perfectly matched between the h-BN and r-BN crystallites. Fig. 1 also illustrates that these lamellae were quite narrow with spacings as little as two to three lattice fringes. Twinning about the basal planes within the r-BN regions can be recognized as indicated by ▼. It is well known that the basal planes of the sp^2-bonded BN exhibit a large degree of curvature, the *c*-axis of the graphitic BN planes being mainly parallel to the film/substrate interface. The present observation agrees well with these previous results [3, 5]. The area of interface in Fig. 1 that is indicated by an arrow reveals information about the atomic structure of the interface in the sp^2-bonded BN. Two adjacent regions in the upper part of Fig. 1 were oriented close to the common [2110] zone axes and the basal planes were perfectly matched across the interface. It can be seen in Fig. 1(b) that the $(01\bar{1}\bar{1})_{\text{r-BN}}$ plane was parallel to the $(01\bar{1}2)_{\text{r-BN}}$ plane, and the $(01\bar{1}\bar{1})_{\text{r-BN}}$ plane was close to the $(10\bar{1}0)_{\text{h-BN}}$ plane. Thus, the following orientation relationship between the h-BN and r-BN phases was deduced:

$$\text{OR-2:}\ [2\bar{1}\bar{1}0]_{\text{h-BN}}\|[2\bar{1}\bar{1}0]_{\text{r-BN}}$$
$$(01\bar{1}\bar{0})_{\text{h-BN}}\|(01\bar{1}\bar{1})_{\text{r-BN}}$$

Both the orientation relationship and the parallelism between $(01\bar{1}\bar{1})_{\text{r-BN}}$ and $(01\bar{1}2)_{\text{r-BN}}$ planes suggest that the grain boundary energy was relatively low. Note that simulated images, which are shown in Fig. 1(c), are in excellent agreement with the experimental ones.

Fig. 2(a) is a cross-sectional HRTEM micrograph showing the structure of sp^2-bonded BN in film 2, where the periodicities within the basal planes were also visible. Specific areas were sufficiently well aligned with a $\langle 2\bar{1}\bar{1}0\rangle$ direction. Schematic key diagrams showing the angles between sets of fringes for these areas are presented in Fig. 2(b). It can be seen that most of the sp^2-bonded BN was in the r-BN configuration. The grain boundaries within the sp^2-bonded BN indicated as A and C in Fig. 2(a) can be recognized. Their simulated images are inserted in

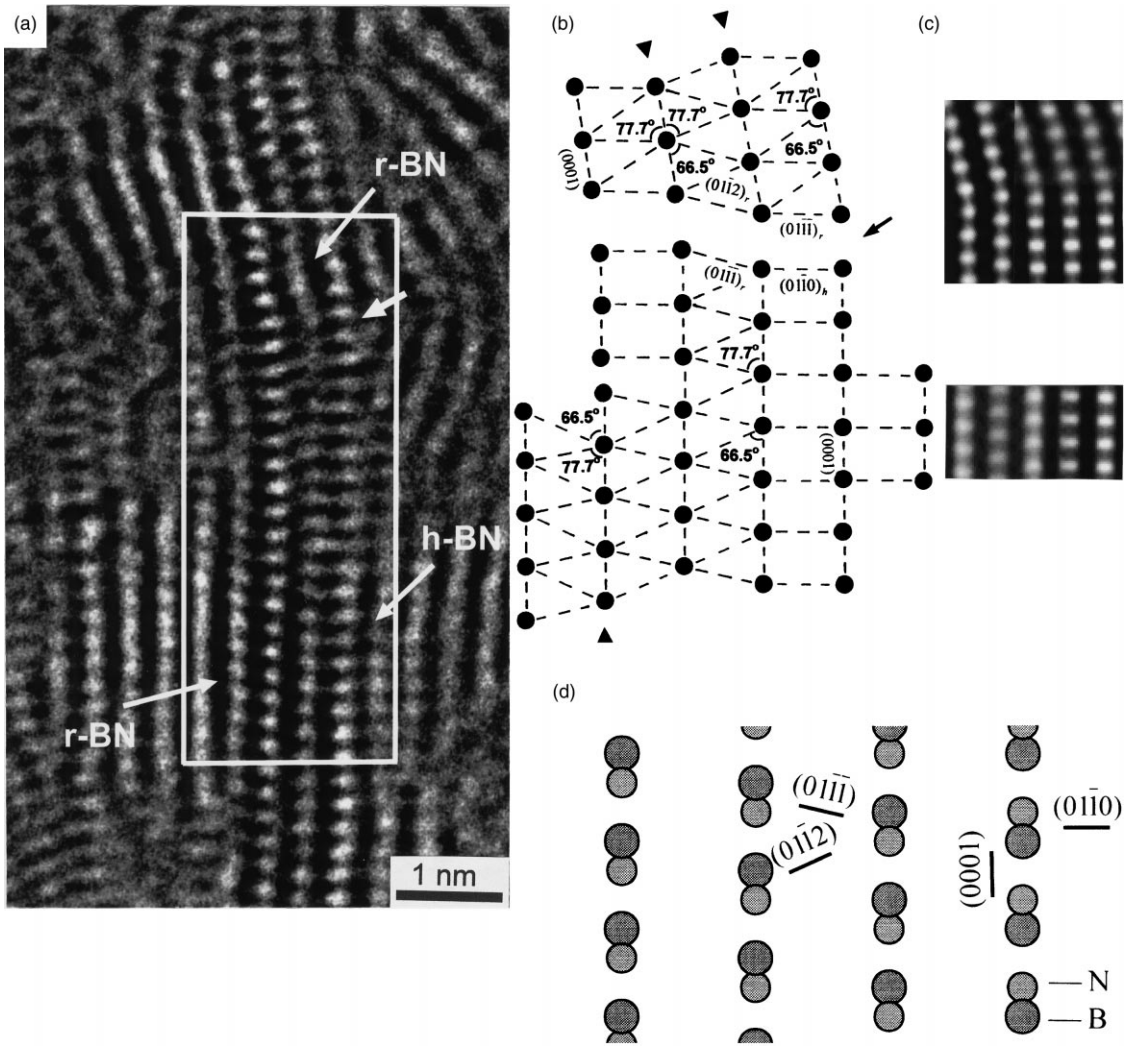

Fig. 1. (a) Cross-sectional HRTEM image showing a typical area of sp^2-bonded BN in film 2. (b) Schematic key diagram showing angles between the lines of intense white points within the region surrounded by a white square frame. Number of horizontal fringes in (b) is not coincident with that in (a). (c) Corresponding simulated images (thickness 5 nm, defocus −90 nm). (d) Cross-sectional view of $(0001)_{h\text{-}BN}\|(0001)_{r\text{-}BN}$ planes. The direction of the incident beam is close to $[2\bar{1}\bar{1}0]$. The direction of film growth is vertically upward.

Fig. 1(a). The present results show that the grain boundary plane in region A was close to the $(01\bar{1}2)_{r\text{-}BN}\|(0\bar{1}11)_{r\text{-}BN}$ plane and the grain boundary plane in region C was close to the $(0\bar{1}11)_{r\text{-}BN}\|(01\bar{1}0)_{h\text{-}BN}$ plane, in keeping with the results reported above. Note that r-BN twins on the $\{0\bar{1}11\}_{r\text{-}BN}$ planes were occasionally observed.

Edge dislocations are common within turbostratic BN and lead to strong local bending of the t-BN atomic planes. An HRTEM micrograph of such a region is shown in Fig. 3(a). h-BN and r-BN crystallites were identified from the angles of the lattice fringes, and a schematic key diagram showing the possible atomic arrangement within the region surrounded by a white frame is presented in Fig. 3(b). It can be seen that the sp^2-bonded BN material consisted of small regions forming in a layered manner normal to the film growth direction and consisting of r-BN and h-BN lamellae. Both phases grew by such a way that the $(01\bar{1}2)_{r\text{-}BN}$, $(01\bar{1}1)_{r\text{-}BN}$ and $(01\bar{1}0)_{h\text{-}BN}$ planes were almost parallel, resulting in good coherency between the crystallites. Thus, the third orientation relationship between the r-BN and h-BN phases can be expressed as follows:

$$\text{OR-3:}\quad \begin{matrix}[2\bar{1}\bar{1}0]_{h\text{-}BN}\|[2\bar{1}\bar{1}0]_{r\text{-}BN}\\ (01\bar{1}0)_{h\text{-}BN}\|(01\bar{1}2)_{r\text{-}BN}\end{matrix}.$$

The results presented here are the first experimental observations showing that the sp^2-bonded BN consists of r-BN and h-BN lamellae obeying specific orientation relationships. Both phases coexist together in

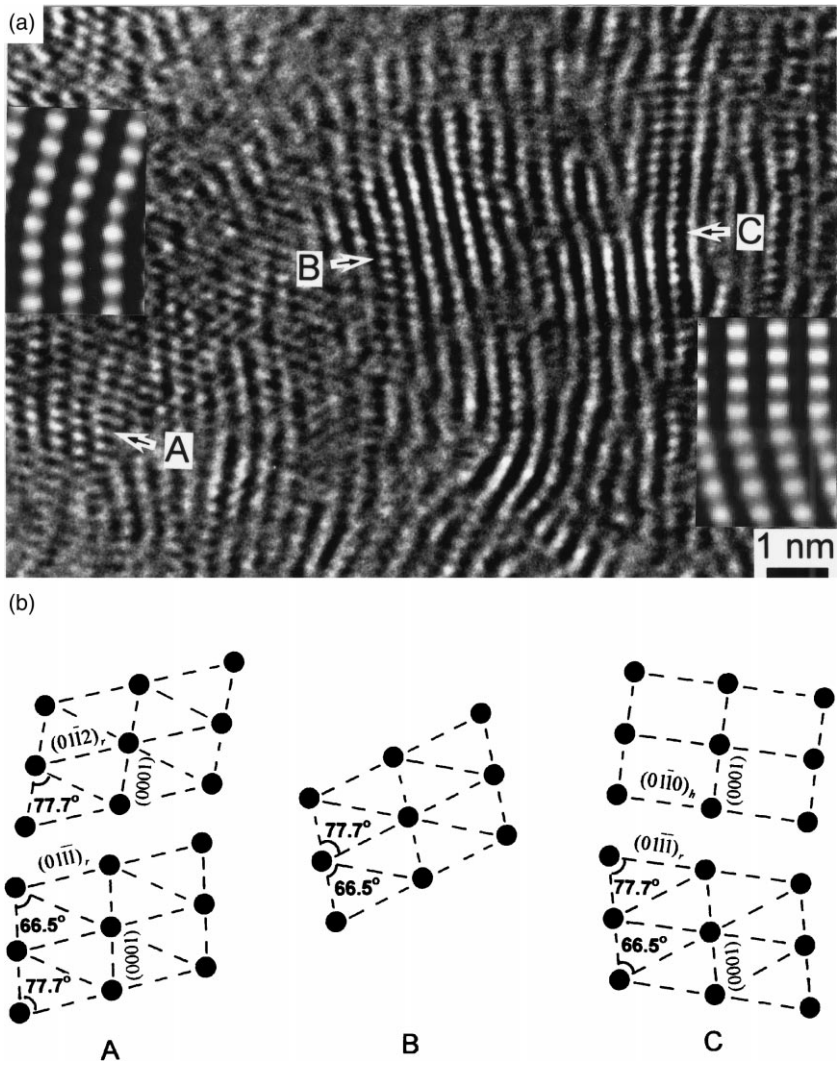

Fig. 2. (a) Cross-sectional HRTEM image of film 2 and (b) its schematic key diagram showing angles between sets of fringes in the regions indicated as A, B and C in (a). Microstructure shows that most part of the sp^2-bonded BN material is in the r-BN configuration. The direction of the incident beam is close to $[2\bar{1}\bar{1}0]$. The calculated images (enlarged) for zones A and C are inserted (thickness 5 nm, defocus −90 nm).

the turbostratic layer of the c-BN films. The observed periodicities within the basal planes and measured fringe angles are strongly supportive of the formation of narrow lamellae in either the r-BN or the h-BN configuration. The present results support the conclusion of Thomas *et al*. [40] who suggested that the basal planes of turbostratic BN have a random rotational stacking so that the material is not truly in a long-range hexagonal configuration. The observed *d* spacings in the present study were consistent with the value of 0.33 nm, which is characteristic of the r-BN and h-BN phases. This is in keeping with the experimental data of Zhou *et al*. [8] but it is, however, in contradiction with the data of Yamada-Takamura *et al*. [10] and Medlin *et al*. [5], who reported that the spacing of the basal planes is typically larger in the turbostratic material than in ordered, crystalline material. Note that in the present study the larger values were measured near the core regions of dislocations within the sp^2-bonded BN, where severe distortion and bending were frequently observed.

Yamada-Takamura *et al*. [10] and Medlin *et al*. [4] suggested that sp^2-bonded BN grows with a layered structure consisting of h-BN layer first, followed by r-BN layer at the c-BN nucleation sites. These results were not confirmed in the present study. Thorough TEM observation showed that the structure of turbostratic BN contained a mixture of r-BN and h-BN phases throughout the depth of the films. Note that we observed the r-BN crystallites near a thin amorphous layer just 4 nm away from the Si/BN interface.

Many reports in the literature [2,3,5,6,10] have shown that sp^2-bonded BN has a characteristic orientation of its basal planes, which are oriented orthog-

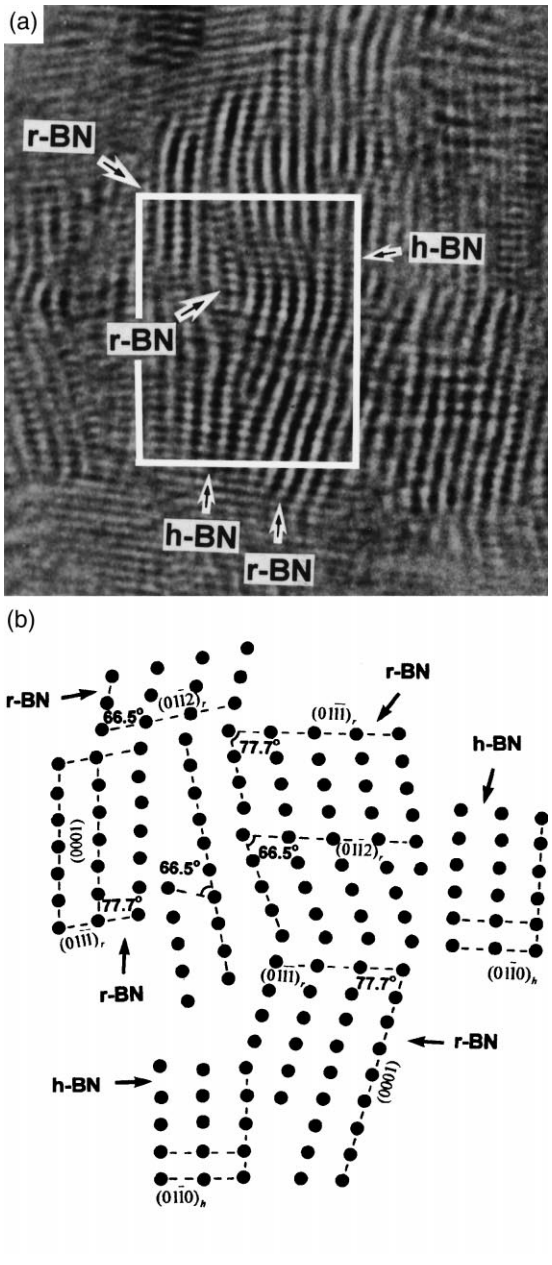

Fig. 3. (a) Cross-sectional HRTEM image of film 2 and (b) its schematic key diagram showing that the sp^2-bonded BN material consists of small regions forming in a layered manner normal to the film growth direction and consisting of r-BN and h-BN crystallites. The direction of the incident beam is close to [2110]. The direction of film growth is vertically upward.

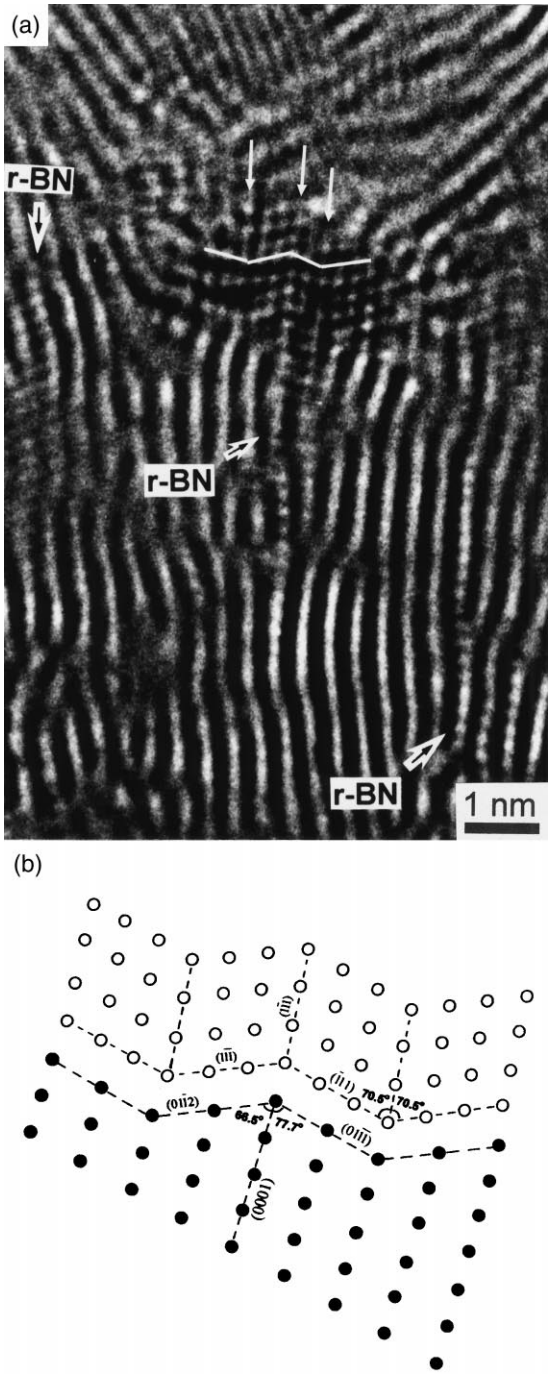

Fig. 4. (a) Cross-sectional HRTEM image showing the interface between the highly twinned c-BN crystallite and its sp^2-bonded BN precursor. Arrows show the twinning planes of c-BN and the other sets of $\{111\}_{c\text{-}BN}$ planes are indicated by white lines. (b) Schematic key diagram showing the probable matching of atomic planes on the grain boundary. The direction of the incident beam is close to $[\bar{2}110]_{r\text{-}BN} \| \langle 110 \rangle_{c\text{-}BN}$. The direction of film growth is vertically upward.

onal to the film/substrate interface. Although our observation is in keeping with these previous results, graphitic basal planes tilted around an axis lying in the plane of the film were also observed. Cardinale *et al*. [12] showed that the most stable orientation calculated for the h-BN crystals differs from that observed experimentally. They suggested that the complex microstructure of the graphitic BN is not adequately described by the single-crystal h-BN calculation. The present results support their conclusion.

3.2. Nucleation and growth of c-BN crystallites

Fig. 4(a) shows a c-BN crystal with a grain size of 2 nm located 20 nm away from the film/substrate interface and oriented along a ⟨110⟩ zone axis. There-

fore, both sets of {111} planes are visible, one of them being almost parallel to the basal planes of the graphitic boron nitride. The c-BN crystal was highly twinned with the width of twin lamellae equal to a spacing of four fringes. Only twinning about a single type of {111} plane was observed and this finding agrees well with the previous results [5]. It is important to note that the twin planes of c-BN were almost parallel to the basal planes of sp^2-bonded BN. A crystallographic alignment between the basal planes of graphitic boron nitride and the {111} planes of c-BN has been reported [10, 16], but this is the first experimental observation showing that the basal planes form parallel with the c-BN twin planes. Within a specific area near the interface between the c-BN and sp^2-bonded BN, a two-dimensional lattice image of the graphitic BN was seen as marked by the arrow. Angles between sets of fringes indicate that this local part of the sp^2-bonded BN material was in the r-BN configuration. Fig. 4(b) is a schematic key diagram showing the probable matching of atomic planes between the c-BN and r-BN crystallites on the grain boundary. It can be seen that one of the sets of $\{111\}_{c\text{-}BN}$ planes within every twinned c-BN crystallite was parallel to either the $(01\bar{1}1)_{r\text{-}BN}$ or the $(01\bar{1}2)_{r\text{-}BN}$ plane of the r-BN phase. Thus, the following orientation relationships between the c-BN and r-BN phases were deduced:

OR-I: $[\bar{2}110]_{r\text{-}BN} \| [110]_{c\text{-}BN}$
$(01\bar{1}\bar{1})_{r\text{-}BN} \| (\bar{1}11)_{c\text{-}BN}$ (interface plane)
$(0001)_{r\text{-}BN} \approx \| (1\bar{1}1)_{c\text{-}BN}$

OR-II: $[\bar{2}110]_{r\text{-}BN} \| [\bar{1}\bar{1}0]_{c\text{-}BN}$
$(01\bar{1}2)_{r\text{-}BN} \| (1\bar{1}\bar{1})_{c\text{-}BN}$ (interface plane)
$(0001)_{r\text{-}BN} \approx \| (1\bar{1}\bar{1})_{r\text{-}BN}$

They are simply related by a rotation of 180° about their common axis $[0001]_{r\text{-}BN} \| [1\bar{1}1]_{c-BN}$, although the interface planes are quite different. Fig. 4 shows that every third $(111)_{c\text{-}BN}$ plane closely matched with every alternate $(0001)_{r\text{-}BN}$ plane in accordance with previous results [10, 16]. This finding implies that the interface was semicoherent. Note that to some extent this orientation relationship is similar to that reported by Li *et al.* [42] in which the diamond (111) planes were parallel to the graphite (0001) planes, and the diamond $[1\bar{1}0]$ direction was parallel to the graphite $[11\bar{2}0]$ direction. Fig. 4 also demonstrates that, upon nucleation, the c-BN crystallite did not continue to grow but transformed into the sp^2-bonded BN. This result suggests that the optimum conditions for both nucleation and growth may be different and must be discussed separately [30].

Fig. 5 is just one more example showing that alignment between the {111} twin planes of c-BN phase and the basal planes of sp^2-bonded BN was prevalent. Medlin *et al.* [5] suggested that the twinning observed

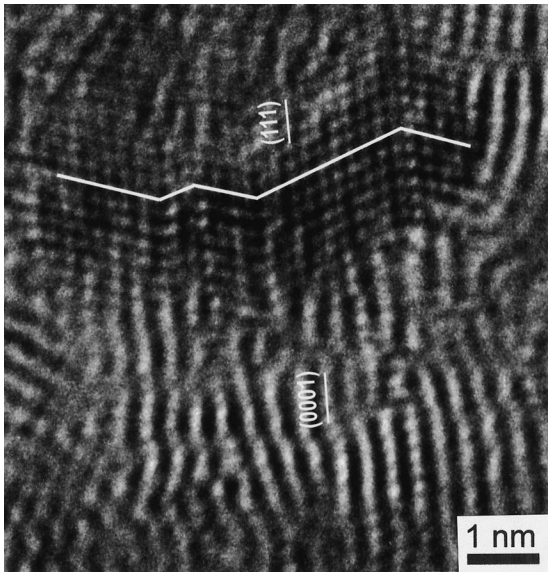

Fig. 5. Cross-sectional HRTEM image showing alignment between the {111} twin planes of the c-BN crystallite and the basal planes of the sp^2-bonded BN. The direction of the incident beam is close to $<110>_{c\text{-}BN}$. The direction of film growth is vertically upward.

in the c-BN films reflects the original stacking sequence of the turbostratic material. The present results do not appear to support their interpretation. In contrast, the formation of highly twinned c-BN crystallites with twinning occurring about a single type of {111} plane is thought to assist in good atomic matching between the $(111)_{c\text{-}BN}$ close-packed planes of the c-BN phase and the $(01\bar{1}\bar{2})_{r\text{-}BN}$ and $(01\bar{1}\bar{1})_{r\text{-}BN}$ planes of the r-BN phase. Therefore, it would be expected that this good atomic matching yields a low interface energy.

The orientation relationships between the c-BN and sp^2-bonded BN can be investigated further. The HRTEM micrograph of Fig. 6 shows the atomic structure of the interface between the sp^2-bonded BN and c-BN crystallites 30 nm away from the film/substrate interface. Note that in this particular case the basal planes of graphitic BN were not orthogonal to the substrate surface, contradicting previous results [2,3,5,6,10]. The interface area was sufficiently well aligned with the $[110]_{c\text{-}BN} \| [\bar{2}110]_{t\text{-}BN}$ direction. Within the sp^2-bonded BN, both r-BN and h-BN lamellae can be recognized [see Fig. 6(b)]. Their basal planes were parallel and deviated about 2.5° from the $(1\bar{1}1)_{c\text{-}BN}$ plane. The $(1\bar{1}\bar{1})_{c\text{-}BN}$ plane was almost parallel to the $(01\bar{1}2)_{r\text{-}BN}$ plane and the $(001)_{c\text{-}BN}$ plane was close to the $(01\bar{1}2)_{h\text{-}BN}$ plane. Thus, the following orientation relationships were fulfilled within a few degrees

OR-II: $[110]_{c\text{-}BN} \| [2\bar{1}\bar{1}0]_{r\text{-}BN}$
$(1\bar{1}\bar{1})_{c\text{-}BN} \| (01\bar{1}2)_{r\text{-}BN}$ (interface plane)
$(1\bar{1}1)_{c\text{-}BN} \| (0001)_{r\text{-}BN}$

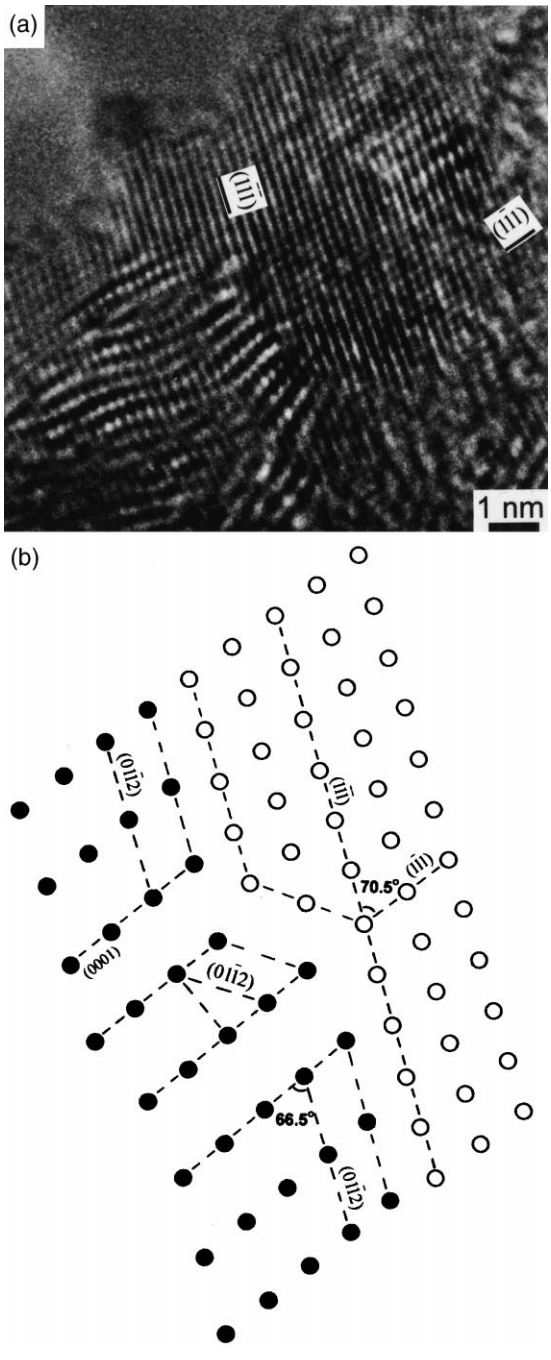

Fig. 6. (a) Cross-sectional HRTEM image showing a single grain boundary between the c-BN crystallite and the sp^2-bonded BN region. (b) Schematic key diagram showing the matching of atomic planes on the grain boundary. The direction of the incident beam is $[110]_{c\text{-}BN}\|[2\bar{1}\bar{1}0]_{r\text{-}BN}\|[2\bar{1}\bar{1}0]_{h\text{-}BN}$.

$$[110]_{c\text{-}BN}\|[2\bar{1}\bar{1}0]_{h\text{-}BN}$$
$$(001)_{c\text{-}BN}\|(01\bar{1}2)_{h\text{-}BN}\ \text{(interface plane)}$$
$$(1\bar{1}1)_{c\text{-}BN}\|(0001)_{h\text{-}BN}$$

3.3. Structure of grain boundaries in c-BN film

The structure of grain boundaries was studied in the c-BN layer with a high cubic fraction and up to 70 nm thick. Fig. 7 shows an HRTEM image of a typical region in film 2 taken 30 nm away from the film/substrate interface. This region consisted of a number of c-BN crystallites with a grain size of 5–10 nm oriented along a ⟨110⟩ zone axis. Similar to diamond [37–39], twinning about more than one of the sets of {111} planes was observed and indicated by arrows. Note that the twin planes were not orthogonal to the substrate surface as observed in Fig. 4. Thus, the microstructure of the c-BN crystallites further away from the interfacial sp^2-bonded BN was different from that near the top of the graphitic BN layer.

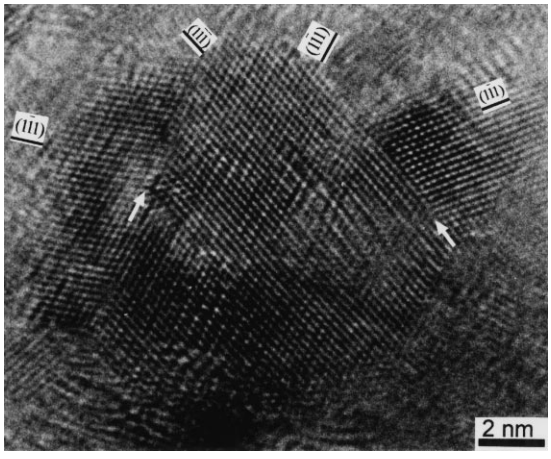

Fig. 7. Cross-sectional HRTEM image of film 2 showing different sets of $\{111\}_{c\text{-}BN}$ twin boundaries. The direction of the incident beam is $[110]_{c\text{-}BN}$.

Two c-BN grains in Fig. 8 were oriented close to a common ⟨110⟩ zone axis and the lattice fringes in both grains were from the {111} planes. Across the interface, $(\bar{1}\bar{1}1)_{c\text{-}BN}$ and $(\bar{1}11)_{c\text{-}BN}$ planes were perfectly matched between the cubic crystallites but their $(1\bar{1}\bar{1})_{c\text{-}BN}$ planes were inclined by about 7°, thus an extra half $(1\bar{1}\bar{1})_{c\text{-}BN}$ plane was visible (shown by an arrow). In Fig. 8, two $\langle 2\bar{1}\bar{1}0\rangle$-oriented r-BN grains within the sp^2-bonded BN region located at the interface between the c-BN crystallites can be recognized. One of the sets of $\{111\}_{c\text{-}BN}$ planes of each of the c-BN grains was almost parallel to the $\{0001\}_{r\text{-}BN}$ plane of the r-BN crystallites, and the $(\bar{1}\bar{1}1)_{c\text{-}BN}$ planes were close to $(01\bar{1}2)_{r\text{-}BN}$ and $(01\bar{1}\bar{1})_{r\text{-}BN}$ planes, respectively. Thus, the orientation relationships between the r-BN and c-BN crystallites were deduced to be

OR-I: $[\bar{1}\bar{1}0]_{c\text{-}BN}\|[\bar{2}110]_{r\text{-}BN}$
$(\bar{1}11)_{c\text{-}BN}\approx\|(0001)_{r\text{-}BN}$
$(1\bar{1}\bar{1})_{c\text{-}BN}\approx\|(01\bar{1}\bar{1})_{r\text{-}BN}$

OR-II: $[110]_{c\text{-}BN}\|[\bar{2}110]_{r\text{-}BN}$
$(1\bar{1}\bar{1})_{c\text{-}BN}\approx\|(0001)_{r\text{-}BN}$
$(1\bar{1}1)_{c\text{-}BN}\|(01\bar{1}2)_{r-BN}$

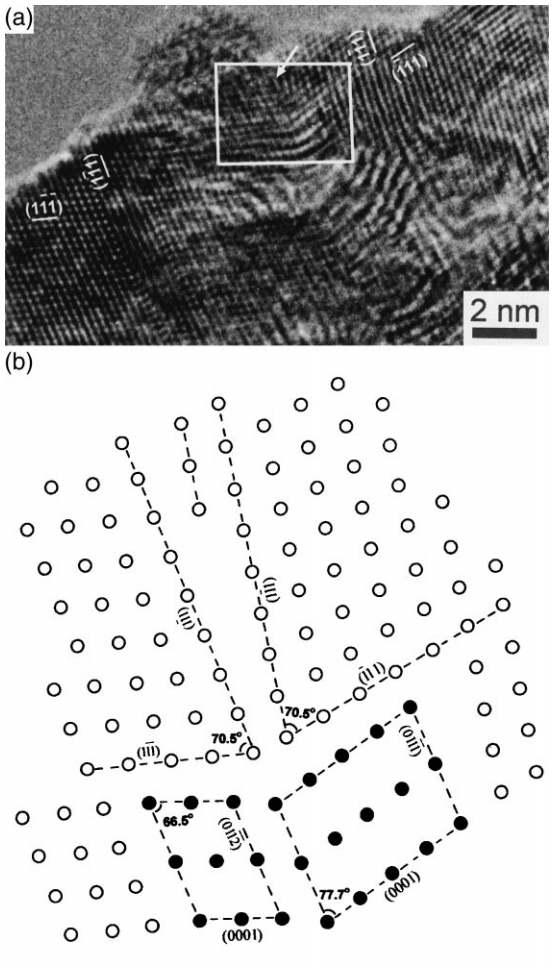

Fig. 8. (a) Cross-sectional HRTEM image of film 2 showing the r-BN region at the boundary of c-BN grains. (b) Schematic key diagram showing the matching of atomic planes between sp^2-bonded BN and c-BN crystallites within the region surrounded by a white square frame. The direction of the incident beam is $[110]_{c\text{-}BN}\|[\bar{1}10]_{c\text{-}BN}\|[\bar{2}110]_{r\text{-}BN}$.

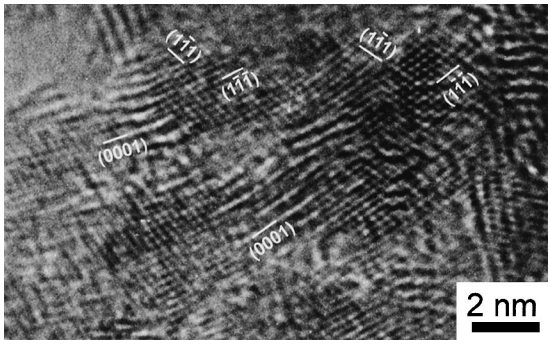

Fig. 9. Cross-sectional HRTEM micrograph of film 2 showing the lattice image of the graphitic basal planes at the boundary between c-BN crystals. The direction of the incident beam is $[110]_{c\text{-}BN}$.

Note that, in this particular case, the atomic matching on grain boundaries consisted of both the $\{111\}_{c\text{-}BN}\|\{0001\}_{r\text{-}BN}$ plane-on-plane matching and the $\{111\}_{c\text{-}BN}\|\{0001\}_{r\text{-}BN}$ edge-to-edge matching. The present TEM observation suggests that the grain boundary energy between cubic grains was relatively high and there was intergranular precipitation of the r-BN phase to reduce the grain boundary energy. The observation that the second phase is precipitated at the interface between the c-BN crystallites agrees well with some recent papers [8, 43].

Fig. 9 is further evidence showing that the atomic structure of a grain boundary depends on the orientation relationship between adjacent grains and the boundary inclination. Several c-BN grains oriented close to the $[110]_{c\text{-}BN}$ zone axis with a size of 3–5 nm can be observed. The boundary planes inclined a few degrees from the $\{111\}_{c\text{-}BN}$ close-packed planes of adjacent c-BN grains. Thus, a thin layer, 1–2 nm, of sp^2-bonded BN was observed between the grains, the basal planes being almost parallel to the other set of $\{111\}_{c\text{-}BN}$ planes. This indicates that the sp^2-bonded layer was probably formed as an intergranular precipitation to reduce the interfacial energy.

Finally, it should be noted that the resolution of most pictures presented here was insufficient, making the exact position of each atomic row at the interface ambiguous. Therefore, the presence and precise location of pores, facets and misfit dislocations at the interface could not be determined.

3.4. Optimum conditions for c-BN nucleation and growth

The structure of the c-BN films was studied using cross-sectional HRTEM images. All films showed the layered structure in accordance with previous results [3,5,6,10]. No c-BN phase was present in film 4 deposited at bias voltage $U_{bias}=-400$ V. This film had a 3 nm amorphous layer, followed by a layer of preferentially oriented sp^2-bonded BN. Film 1, deposited under the lowest bias voltage condition, consisted of a thick region of sp^2-bonded BN, but only traces of the c-BN phase were detected by a selected-area electron diffraction (SAED). The synthesis of c-BN films with a high cubic fraction was achieved when the bias voltage was kept constant at -300 V. A typical cross-sectional bright-field image, a dark-field image using a 111 c-BN reflection and a SAED pattern of film 3 are shown in Fig. 10. It can be seen that the most part of the film corresponded to a layer of cubic boron nitride. Thus, in agreement with the previous results [22], c-BN deposition was observed to occur in a window of bias voltage values, all other conditions being the same. A change in the target power also affected the structure of c-BN films. Fig. 11(a) and (b) presents cross-sectional HRTEM micrographs showing the atomic structure near the film/substrate interface in films 3 and 2, respectively. The incident beam direction is $[110]_{Si}$. The deposition rate of film 3 was

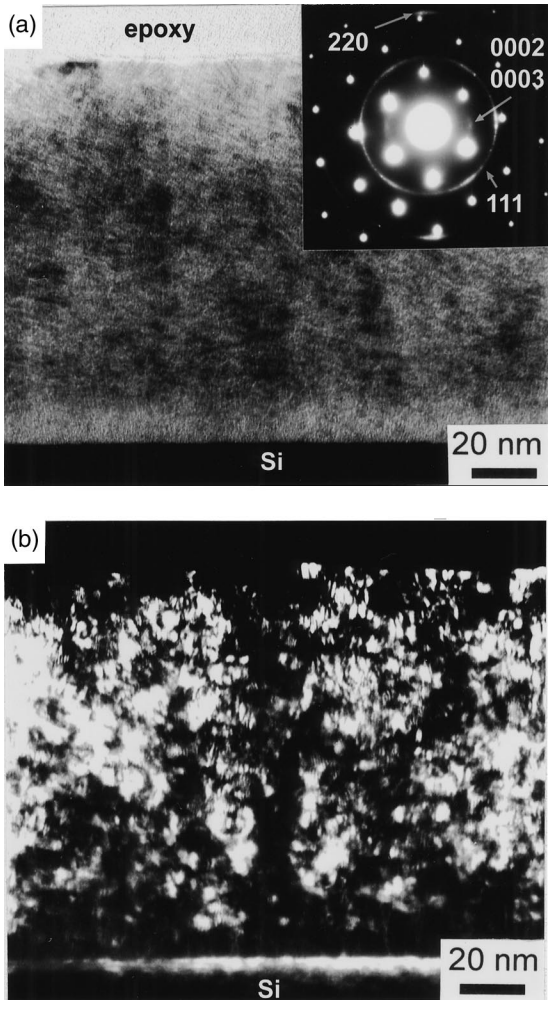

Fig. 10. (a) Cross-sectional bright-field TEM image and (b) dark-field image using a 111 c-BN reflection showing a ~110 nm thick c-BN film with a SAED pattern inset.

higher than that of film 2 (see Table 1), thus film 3 was deposited under softer ion bombardment conditions. Film 3 had a ~5 nm amorphous layer, followed by ~10 nm of oriented sp^2-bonded BN, and the layer of c-BN over them. Fig. 11(a) illustrates that c-BN nucleation occurred preferentially on the concave surface on the sp^2-bonded BN layer just 10 nm away from the substrate surface (shown by an arrow). Therefore, it is reasonable to assume that c-BN nucleated in surface regions with a high level of local stress. Fig. 11(b) shows a c-BN crystallite with a grain size of about 12 nm nucleated 9 nm away from the substrate surface in film 2 deposited under the high ratio of bombardment ions to deposition atoms. In this particular case the c-BN/t-BN interface was almost flat. In film 2, the critical thickness of the intermediate sp^2-bonded BN layer was smaller in comparison with that in film 3. It is well known that the growth of BN films is accompanied by an increase in compressive stress. It has been shown by Zeitler *et al.* [13] that compressive stress is increased with increasing ion-to-atom arrival ratio. Therefore, this insufficient stress within the growing film was probably compensated by the more intensive ion bombardment. Note that the transition from sp^2-bonded BN to single-phase cubic BN occurred at varying thickness in the same film. In film 2, the sp^2-bonded BN layer was observed to grow up to a thickness of 35 nm until the surface was completely covered by the c-BN layer. The question of whether it is possible to grow a pure c-BN film, not a mixed phase, is still open. As was shown in Section 3.3, the grain boundaries in the upper layer of the BN films consisted of both coincidence c-BN boundaries and intergranular precipitates of sp^2-bonded BN. Finally note that a thin h-BN surface layer on top of the c-BN film, as reported by Park *et al.* [44], was not observed in the present study.

4. DISCUSSION

4.1. Crystallography

In the present study, the crystallography and the atomic structure of the interfaces between BN crystallites were studied. The experimental observations described above can be summarized as follows.

1. The sp^2-bonded BN material consisted of small regions, 1–5 nm thick, formed in a layered manner parallel to the substrate surface and consisted of parallel lamellae in both h-BN and r-BN configurations. Such a structure is often referred to as "turbostratic" [40]. It should be noted that some sp^2-bonded BN regions could not be fully classified as either a hexagonal or a rhombohedral structure. Although the angles between sets of fringes in such regions were consistent with those for the r-BN structure, only the two-layer stacking instead of a three-layer stacking sequence, which is characteristic of the rhombohedral phase, was observed. This result implies that the plane stacking in the turbostratic BN is random, in keeping with the conclusion by Thomas *et al.* [40], although the local symmetry between the neighboring basal planes is described well by either the hexagonal or the rhombohedral configuration.
2. Because of the effect of crystallography during the growth of c-BN films, specific orientation relationships were maintained between the c-BN, r-BN and h-BN phases, resulting in a good coherency. Three specific orientation relationships were found to exist between the h-BN and r-BN phases

$$\text{OR-1:}\quad [2\bar{1}\bar{1}0]_{\text{h-BN}} \| [2\bar{1}\bar{1}0]_{\text{r-BN}}$$
$$(0001)_{\text{h-BN}} \| (0001)_{\text{r-BN}}$$

$$\text{OR-2:}\quad [2\bar{1}\bar{1}0]_{\text{h-BN}} \| [2\bar{1}\bar{1}0]_{\text{r-BN}}$$
$$(01\bar{1}0)_{\text{h-BN}} \| (01\bar{1}\bar{1})_{\text{r-BN}}$$

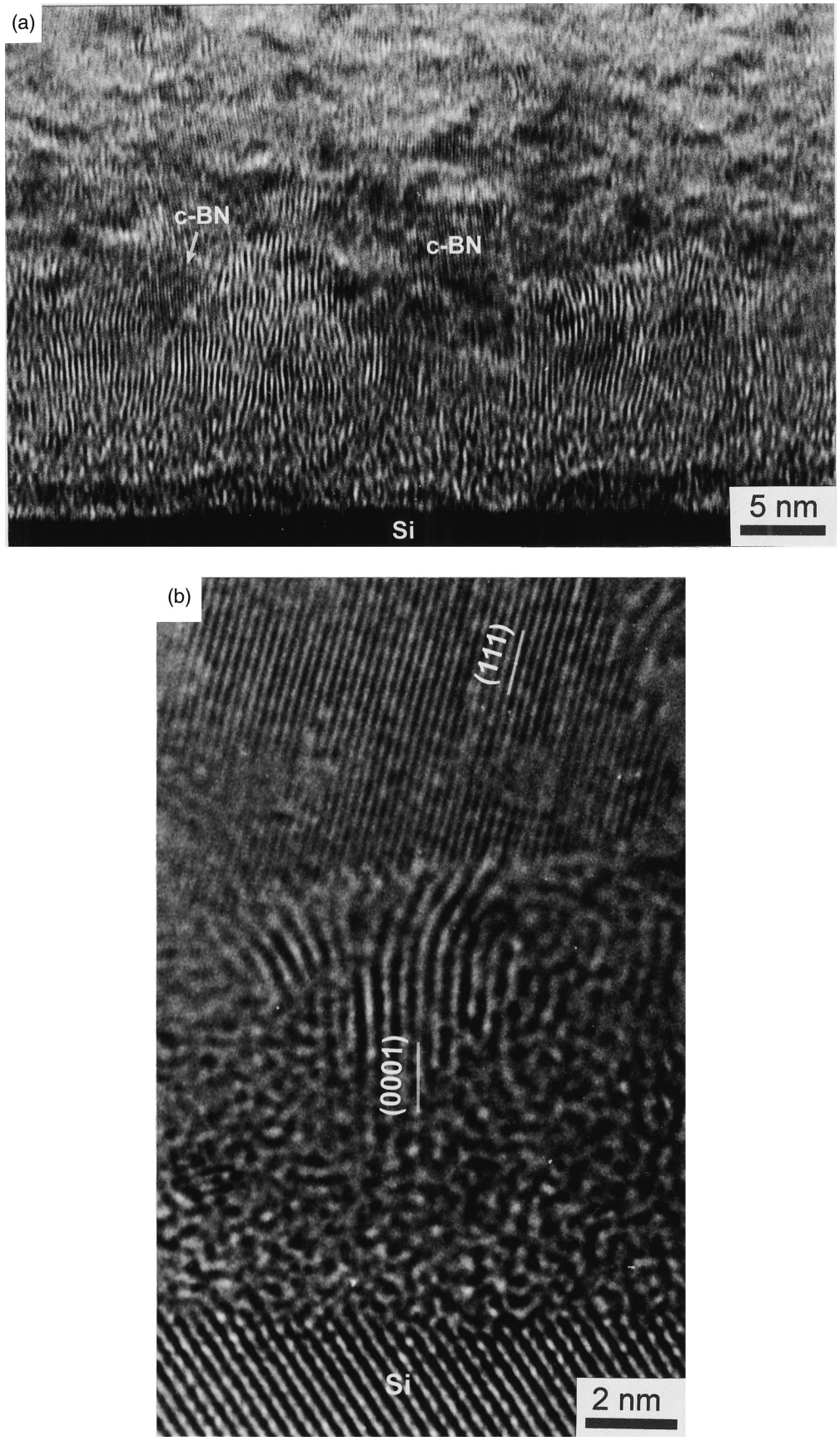

Fig. 11. Cross-sectional TEM micrographs showing traces of $(111)_{c\text{-}BN}$ and $(0001)_{t\text{-}BN}$ planes in (a) film 3 and (b) film 2.

OR-3: $[2\bar{1}\bar{1}0]_{\text{h-BN}}\|[2\bar{1}\bar{1}0]_{\text{r-BN}}$
$(01\bar{1}\bar{0})_{\text{h-BN}}\|(01\bar{1}\bar{2})_{\text{r-BN}}$

The r-BN crystallites in the adjacent sp^2-bonded regions were frequently observed to grow in such a way that the grain boundary plane was parallel to the $(01\bar{1}\bar{2})_{\text{r-BN}}\|(01\bar{1}\bar{1})_{\text{r-BN}}$ plane. Twinning about both the basal planes and the $\{01\bar{1}\bar{1}\}_{\text{r-BN}}$ planes within r-BN phase was frequently observed. Note that the sp^2-bonded BN material formed preferentially in the r-BN configuration.

3. The oriented t-BN, consisting of the h-BN and r-BN lamellae, acted as a structural precursor for c-BN formation. Both structural constituents of the turbostratic BN were found to obey specific orientation relationships with the c-BN

OR-I: $[\bar{2}110]_{\text{r-BN}}\|[110]_{\text{c-BN}}$
$(01\bar{1}\bar{1})_{\text{r-BN}}\|(\bar{1}11)_{\text{c-BN}}$ (interface plane)
$(0001)_{\text{r-BN}}\approx\|(1\bar{1}\bar{1})_{\text{c-BN}}$

OR-II: $[\bar{2}110]_{\text{r-BN}}\|[\bar{1}\bar{1}0]_{\text{c-BN}}$
$(01\bar{1}\bar{2})_{\text{r-BN}}\|(1\bar{1}\bar{1})_{\text{c-BN}}$ (interface plane)
$(0001)_{\text{r-BN}}\approx\|(1\bar{1}\bar{1})_{\text{c-BN}}$

$[2\bar{1}\bar{1}0]_{\text{h-BN}}\|[110]_{\text{c-BN}}$
$(01\bar{1}\bar{2})_{\text{h-BN}}\|(001)_{\text{c-BN}}$ (interface plane)
$(0001)_{\text{h-BN}}\|(1\bar{1}\bar{1})_{\text{c-BN}}$

This result implies that the c-BN/r-BN and c-BN/h-BN interfaces were semicoherent.

4. The c-BN crystallites possessed an in-plane $\langle 110\rangle$ texture, the $[110]_{\text{c-BN}}$ direction being parallel to $[110]_{\text{Si}}$. In the c-BN region adjacent to the sp^2-bonded BN layer, the c-BN crystallites were oriented with at least one $\langle 111\rangle$ direction lying in the plane of the film, in keeping with previous results [16]. The c-BN crystallites were highly twinned. Within a single c-BN crystallite adjacent to the sp^2-bonded BN layer twinning about a single type of $\{111\}$ plane was observed, the twin planes being parallel to the basal planes of t-BN. In the c-BN films further away from the sp^2-bonded BN layer, twinning about more than one of the sets of $\{111\}$ planes was observed.
5. It is suggested that the structure and crystallography of the c-BN layer were directly related to the structure and the preferential orientation of the sp^2-bonded BN layer. The present results support the conclusion by Cardinale *et al.* [12] that the c-BN texture would arise directly from the mechanism of growth rather than the minimization of elastic strain energy. Thus, a direct transformation from h-BN to c-BN causing a localized melting of small regions (the so-called "thermal spike"), suggested by McKenzie *et al.* [11], is questionable. In contrast, favorable crystallographic and interface energy relationships appear to result in the texture of the c-BN.

An alternative model of the origin of the c-BN texture suggested by Medlin *et al.* [4, 5] is that the transformation occurs through the rhombohedral form of boron nitride under local compressive stress. Because of the structural similarities between the r-BN and c-BN phases, the r-BN to c-BN pathway is preferable compared with the reconstructive process necessary to directly convert the hexagonal phase. In this contest, one special feature of the orientation relationships observed should be mentioned. Every alternate basal plane of the sp^2-bonded BN was closely matched with a corresponding $\{111\}_{\text{c-BN}}$ plane. Since the stacking of the alternate h-BN basal planes is similar to that of the $\{111\}_{\text{c-BN}}$ planes, c-BN can directly nucleate on the edges of the oriented basal planes of h-BN in a semicoherent manner.

The rationality of the orientation relationships between c-BN and both sp^2-bonded constituents observed in the present study can be understood by considering the stereographic projection in Fig. 12. It can be seen that each orientation relationship yields a small misorientation between the coincident planes. Note that when the sp^2-bonded BN grows in a layered manner, the basal planes of r-BN and h-BN phases being parallel, OR-II between c-BN and r-BN phases and the orientation relationship between c-BN and h-

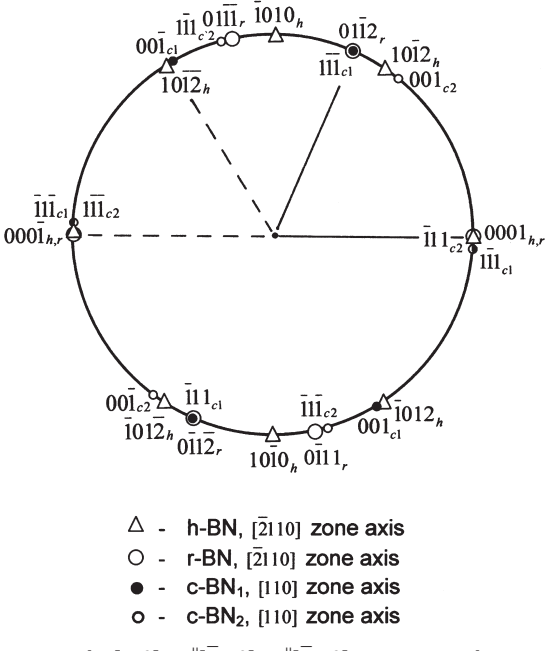

Fig. 12. The $[110]_{\text{c-BN}}\|[\bar{2}110]_{\text{r-BN}}\|[\bar{2}110]_{\text{h-BN}}$ stereographic projection showing a small misorientation between the coincident planes for the orientation relationships observed between the c-BN, r-BN and h-BN phases.

BN phases are fulfilled simultaneously. Thus, it is expected that the interface energy between these phases would be low. The lattice misfits between the coinciding planes of c-BN, r-BN and h-BN phases are summarized in Table 2. It can be seen that even the largest misfit does not exceed 6%.

4.2. c-BN growth mechanism

In the present study the c-BN films grew in the sequence of amorphous BN (a-BN), t-BN and c-BN layers, similar to most of the previous results. An amorphous BN layer appears to be formed either during presputtering or at the beginning of sputtering as a result of ion mixing of B, N and Si. The existence of a critical thickness of sp^2-bonded BN seems to be necessary for c-BN nucleation. The stress is strongly dependent on the film thickness. Thus, it seems reasonable to assume that a defined threshold stress value in the intermediate layer is necessary to form the c-BN phase, in keeping with the compressive stress model suggested by McKenzie *et al.* [11]. Nucleation of the cubic phase was observed to occur at differing thicknesses of the sp^2-bonded BN layer. This result implies that the c-BN crystallites nucleated under different macroscopic film stresses. The complex structure of the turbostratic BN, comprising a large volume fraction of the grain boundaries, is thought to possess both high macroscopic and microscopic film stress. High local stress in the film surface, for example on the concave surface of sp^2-bonded BN, may accelerate the nucleation of cubic phase. Several reports indicated the reduction of ion energy needed for the growth of c-BN after nucleation [45, 46]. It is speculated that once the nucleation of c-BN occurs, it will be able to continue to grow under the same conditions. However, the subsequent transition from c-BN phase to t-BN phase observed in the present study is in contradiction with this conclusion. Since growth of the BN films is connected with an increase in compressive stress [11, 13], the contribution of local stress in the initial nucleation of cubic phase has to be of great importance. When the compressive stress rises, boron nitride film with a high c-BN content is achieved. The intrinsic microstructure of c-BN crystallites and the crystallography between the cubic and graphitic BN phases show that the c-BN phase is directly related to the structure of the precursor phases.

5. SUMMARY

The mechanism and the crystallography of c-BN films grown by RF bias sputtering have been investigated by means of HRTEM. The following results were obtained.

1. The sp^2-bonded BN consisted of small regions, 1–5 nm thick, forming in a layered manner normal to the film growth direction. Each region consisted of parallel lamellae in both the h-BN and r-BN configurations. r-BN crystallites within the turbostratic BN layer often grew in such a way that the $(01\bar{1}2)_{\text{r-BN}} \| (01\bar{1}\bar{1})_{\text{r-BN}}$ plane was parallel to the grain boundary. Twinning about both the basal plane and the $\{01\bar{1}1\}_{\text{r-BN}}$ plane within r-BN phase has been observed. The hexagonal and rhombohedral phases obeyed specific orientation relationships:

   OR-1: $[2\bar{1}\bar{1}0]_{\text{h-BN}} \| [2\bar{1}\bar{1}0]_{\text{r-BN}}$, $(0001)_{\text{h-BN}} \| (0001)_{\text{r-BN}}$;

   OR-2: $[2\bar{1}\bar{1}0]_{\text{h-BN}} \| [2\bar{1}\bar{1}0]_{\text{r-BN}}$, $(01\bar{1}0)_{\text{h-BN}} \| (01\bar{1}1)_{\text{r-BN}}$;

   OR-3: $[2\bar{1}\bar{1}0]_{\text{h-BN}} \| [2\bar{1}\bar{1}0]_{\text{r-BN}}$, $(01\bar{1}0)_{\text{h-BN}} \| (01\bar{1}2)_{\text{r-BN}}$.

2. The c-BN growth was preceded by the formation of a layer of sp^2-bonded BN. Because of the effect of crystallography during c-BN growth, specific orientation relationships were fulfilled between the cubic phase and its hexagonal and rhombohedral precursors:

   OR-I: $[\bar{2}110]_{\text{r-BN}} \| [110]_{\text{c-BN}}$
   $(01\bar{1}\bar{1})_{\text{r-BN}} \| (\bar{1}11)_{\text{c-BN}}$ (interface plane)
   $(0001)_{\text{r-BN}} \approx \| (1\bar{1}1)_{\text{c-BN}}$

Table 2. Lattice misfit between h-BN, r-BN and c-BN planes

$(hkl)_h$	Lattice spacing, d_1 (nm)	$(hkl)_r$	Lattice spacing, d_2 (nm)	$(hkl)_c$	Lattice spacing, d_3 (nm)	$(d_1-d_3)/d_1$	$(d_2-d_3)/d_2$
{0002}	0.333×2=0.666	{0003}	0.333×2=0.666	{111}	0.209×3=0.627	0.058	0.058
{10$\bar{1}$2}	0.182			{200}	0.181	0.005	
{2$\bar{1}\bar{1}$0}	0.125	{2$\bar{1}\bar{1}$0}	0.125	{220}	0.128	−0.024	−0.024
		{01$\bar{1}$1}	0.212	{111}	0.209		0.014
		{01$\bar{1}$2}	0.199	{111}	0.209		−0.050

OR-II: $[\bar{2}110]_{r\text{-}BN} \| [\bar{1}\bar{1}0]_{c\text{-}BN}$
$(01\bar{1}2)_{r\text{-}BN} \| (1\bar{1}\bar{1})_{c\text{-}BN}$ (interface plane)
$(0001)_{r\text{-}BN} \approx \| (1\bar{1}1)_{c\text{-}BN}$

$[2\bar{1}\bar{1}0]_{h\text{-}BN} \| [110]_{c\text{-}BN}$
$(01\bar{1}2)_{h\text{-}BN} \| (001)_{c\text{-}BN}$ (interface plane)
$(0001)_{h\text{-}BN} \| (1\bar{1}1)_{c\text{-}BN}$

.

The c-BN crystallites were highly twinned, the $\{111\}_{c\text{-}BN}$ twin planes being parallel to the graphitic basal planes. Further away from the sp^2-bonded BN layer, twinning about more than one of the sets of $\{111\}_{c\text{-}BN}$ planes has been observed.

3. The atomic structure of an interface was shown to depend on the orientation relationship between adjacent c-BN grains and the boundary inclination. The grain boundaries consisted of twin boundaries when two grains were oriented close to the $[110]_{c\text{-}BN}$ zone axis and the boundary plane was parallel to the $\{111\}_{c\text{-}BN}$ close-packed planes of adjacent grains. However, a thin layer, 1–2 nm, of sp^2-bonded BN formed between the c-BN grains when the boundary plane inclined a few degrees from the $\{111\}_{c\text{-}BN}$ planes of adjacent grains. In the last case the sp^2-bonded BN precipitates are thought to reduce the grain boundary energy.

Acknowledgements—D.S. acknowledges the support of the Japan Society for the Promotion of Science (JSPS) during this work. This work was supported financially by JSPS under the program "Research for the Future" (JSPS-RFTF Grant No. 97R15301).

REFERENCES

1. McKenzie, D. R., Sainty, W. G. and Green, D., *Mater. Sci. Forum*, 1990, **54/55**, 193.
2. McKenzie, D. R., Cockayne, D. J. H., Muller, D. A., Murakawa, M., Miyake, S., Watanabe, S. and Fallon, P., *J. Appl. Phys.*, 1991, **70**, 3007.
3. Kester, D. J., Ailey, K. S., Davis, R. F. and More, K. L., *J. Mater. Res.*, 1993, **8**, 1213.
4. Medlin, D. L., Friedman, T. A., Mirkarimi, P. B., Mills, M. J. and McCarty, K. F., *Phys. Rev. B*, 1994, **50**, 7884.
5. Medlin, D. L., Friedman, T. A., Mirkarimi, P. B., Rez, P., Mills, M. J. and McCarty, K. F., *J. Appl. Phys.*, 1994, **76**, 295.
6. Kester, D. J., Ailey, K. S., Lichtenwalner, D. J. and Davis, R. F., *J. Vac. Sci. Technol.*, 1994, **12**, 3074.
7. Watanabe, S., Mayake, S., Zhou, W., Ikuhara, Y., Suzuki, T. and Murakawa, M., *Appl. Phys. Lett.*, 1995, **66**, 1478.
8. Zhou, W. -L., Ikuhara, Y., Murakawa, M., Watanabe, S. and Suzuki, T., *Appl. Phys. Lett.*, 1995, **66**, 2490.
9. Mirkarimi, P. B., Medlin, D. L., McCarty, K. F., Dibble, D. C., Clift, W. M., Knapp, J. A. and Barbour, J. C., *J. Appl. Phys.*, 1997, **82**, 1617.
10. Yamada-Takamura, Y., Tsuda, O., Ichinose, H. and Yoshida, T., *Phys. Rev. B*, 1999, **59**, 10, 352.
11. McKenzie, D. R., McFall, W. D., Sainty, W. G., Davis, C. A. and Collins, R. E., *Diamond Relat. Mater.*, 1993, **2**, 970.
12. Cardinale, G. F., Medlin, D. L., Mirkarimi, P. B., McCarty, K. F. and Howitt, D. G., *J. Vac. Sci. Technol.*, 1997, **15**, 196.
13. Zeitler, M., Sienz, S. and Rauschenbach, B., *J. Vac. Sci. Technol.*, 1999, **17**, 597.
14. Kester, D. J. and Messier, R., *J. Appl. Phys.*, 1992, **72**, 504.
15. Mirkarimi, P. B., McCarty, K. F., Medlin, D. L., Wolfer, W. G., Friedmann, T. A., Klaus, E. J., Cardinale, G. F. and Howitt, D. G., *J. Mater. Res.*, 1994, **9**, 2925.
16. Medlin, D. L., Friedmann, T. A., Mirkarimi, P. B., Cardinale, G. F. and McCarty, K. F., *J. Appl. Phys.*, 1996, **79**, 3567.
17. McCarty, K. F., *J. Vac. Sci. Technol.*, 1999, **17**, 2749.
18. McKenzie, D. R. and Bilek, M. M. M., *J. Vac. Sci. Technol.*, 1998, **16**, 2733.
19. Ballal, A. K., Salamanca-Riba, L., Taylor, C. A. II and Doll, G. L., *Thin Solid Films*, 1993, **224**, 46.
20. Mirkarimi, P. B., Medlin, D. L., McCarty, K. F. and Barbour, J. C., *Appl. Phys. Lett.*, 1995, **66**, 2813.
21. Mirkarimi, P. B., McCarty, K. F., Cardinale, G. F., Medlin, D. L., Ottesen, D. K. and Johnsen, H. A., *J. Vac. Sci. Technol.*, 1996, **14**, 251.
22. Ichiki, T., Amagi, S. and Yoshida, T., *J. Appl. Phys.*, 1996, **79**, 4381.
23. Roy, R. A., Catania, P., Saenger, K. L., Cuomo, J. J. and Lossy, R. L., *J. Vac. Sci. Technol. B*, 1993, **11**, 1921.
24. Lifshitz, Y., Kasi, S. R. and Rabalais, J. W., *Phys. Rev. B*, 1990, **41**, 10468.
25. Dworschak, W., Jung, K. and Ehrhardt, H., *Thin Solid Films*, 1995, **254**, 65.
26. Robertson, J., Gerber, J., Sattel, S., Weiler, M., Jung, K. and Ehrhardt, H., *Appl. Phys. Lett.*, 1995, **66**, 3287.
27. Uhlmann, S., Frauenheim, T. and Stephan, U., *Phys. Rev. B*, 1995, **51**, 4541.
28. Reinke, S., Kuhr, M., Kulisch, W. and Kassing, R., *Diamond Relat. Mater.*, 1995, **4**, 272.
29. Hackenberger, L. B., Pilione, L. J. and Messier, R., in *Science and Technology of Thin Films*, eds F. C. Matacotta and G. Ottaviani. World Scientific Publishing Co. Pte. Ltd, Singapore, New Jersey, London, Hongkong, 1995.
30. Yoshida, T., *Diamond Relat. Mater.*, 1996, **5**, 501.
31. Yoshida, T., *Diamond Films Technol.*, 1997, **7**, 87.
32. Shanfield, S. and Wolfson, R., *J. Vac. Sci. Technol. A*, 1983, **1**, 323.
33. Ikeda, T., Kawate, Y. and Hirai, Y., *J. Vac. Sci. Technol. A*, 1990, **8**, 3168.
34. Inagawa, K., Watanabe, H., Ohsone, H., Saitoh, K. and Itoh, A., *J. Vac. Sci. Technol. A*, 1987, **5**, 2696.
35. Murakawa, M. and Watanabe, S., *Surf. Coat. Technol.*, 1990, **43/44**, 128.
36. McKenzie, D. R., *J. Vac. Sci. Technol. B*, 1993, **11**, 1928.
37. Ma, G. H. M., Lee, Y. H. and Glass, J. T., *J. Mater. Res.*, 1990, **5**, 2367.
38. Narayan, J., *J. Mater. Res.*, 1990, **5**, 2414.
39. Schechtman, D., Feldman, A., Vaudin, M. D. and Hutchison, J. L., *Appl. Phys. Lett.*, 1993, **62**, 487.
40. Thomas, J., Weston, N. E. and O'Connor, T. E., *J. Am. Chem. Soc.*, 1963, **84**, 4619.
41. Tsuda, O., Yamada, Y., Fujii, T. and Yoshida, T., *J. Vac. Sci. Technol. A*, 1995, **13**, 2843.
42. Li, Z., Wang, L., Suzuki, T., Argoitia, A., Pirouz, P. and Angus, J. C., *J. Appl. Phys.*, 1993, **73**, 711.
43. Mieno, M. and Yoshida, T., *Surf. Coat. Technol.*, 1992, **52**, 87.

44. Park, K. S., Lee, D. Y., Kim, K. J. and Moon, D. W., *J. Vac. Sci. Technol.*, 1997, **15**, 1041.
45. Takahashi, D., Amagi, S. and Yoshida, T., *Appl. Phys. Lett.*, 1997, **70**, 946.
46. McKenzie, D. R., McFall, W. D., Smith, H., Hingiss, B., Boswell, R. W., Durandet, A., James, B. W. and Falconer, I. S., *Nucl. Instrum. Meth. Phys. Res. B*, 1995, **106**, 90.